



Plasma Interactions with the Space Environment in the Acceleration Region: Indications of CME-trailing Reconnection Regions

Elizabeth A. Jensen^{1,2} , Carl Heiles³ , David Wexler⁴ , Amanda A. Kepley⁵ , Thomas Kuiper⁶ , Mario M. Bisi⁷ ,
Deborah Domingue Lorin¹ , Elizabeth V. Kuiper⁸, and Faith Vilas^{1,9}

¹ Planetary Science Institute 1700 East Fort Lowell, Suite 106 Tucson, AZ 85719, USA; ejensen@psi.edu

² ACS Consulting, LLC, USA

³ Astronomy Department, University of California, USA

⁴ University of Southern Queensland, Australia

⁵ National Radio Astronomy Observatory, USA

⁶ Jet Propulsion Laboratory California Institute of Technology, USA

⁷ Science and Technology Facilities Council, UK

⁸ STAR Prep Academy, USA

⁹ National Science Foundation, USA

Received 2018 March 27; revised 2018 May 14; accepted 2018 May 15; published 2018 July 11

Abstract

Coronal mass ejections (CMEs) are sources of major geomagnetic disturbances. On 2013 May 10, a CME crossed the signal path between the *MERCURY SURFACE, SPACE ENVIRONMENT, GEOCHEMISTRY, AND RANGING (MESSENGER)* spacecraft and Earth. Using the *MESSENGER* signal, characteristics of the density, velocity, and magnetic field properties of the crossing plasma were measured. An anomalously strong event occurred in the plasma trailing the CME's passage that correlated with a wave mode conversion, indicating a potential reconnection region. We determine that the plasma following CMEs should be considered when studying how CMEs evolve in interplanetary space and the severity of their geomagnetic impact.

Key words: magnetic reconnection – methods: observational – plasmas – polarization – Sun: coronal mass ejections (CMEs)

1. Introduction

The plasma of the Sun's photosphere roils in an unusual boiling motion, with its unexpected changes in flow caused by interactions with the surrounding magnetic field. This turbulent behavior persists in the subsequent solar wind that is carried along those magnetic field lines that do not close back onto the Sun's surface, remaining open to interplanetary space. Among the closed magnetic field plasma regions, energy is deposited, particularly in solar active regions, creating the conditions for the sudden release and violent ejection of dense coronal plasma in the form of a coronal mass ejection (CME).

Many components of the plasma, such as the magnetic field, particle flux density, particle energy distribution, and even ion composition distribution, vary with time and distance from the Sun. The plasma of a CME behaves in many ways like a fluid, but not at smaller scales and within certain regions such as shocks, where it is specifically a magnetized kinetic gas. The magnetized kinetic gas behavior is critical in the acceleration region between 2 and 15 solar radii, and it is not well understood. Currently, the acceleration region is studied using fluid-based magnetohydrodynamic (MHD) models, initialized by velocity and density data from polarized brightness images and extrapolations from observations made near 1 au (215 solar radii). The magnetic field, the dominant variable accelerating the plasma, is not typically observed. Here, we present the first observation of a CME's magnetic field structure, density, velocity, and post-passage wake activity in the acceleration region (4–6 solar radii). We provide a comparison with current model estimates, examine the validity of models, and discuss the implications for interactions with various types of planetary bodies.

2. Observations

The solar wind has been observed to increase in bulk radial speed to approximately 50 km s^{-1} through the transition region of the atmosphere to the base of the corona (for a discussion see De Pontieu et al. 2017). The height of the base of the corona varies based on plasma conditions; in general it is around 0.25 solar radii above the Sun's surface. The plasma continues to acquire velocity, reaching, on average, 400 km s^{-1} around 10 solar radii, as determined using radio observations (for example, see Wei et al. 2003). The source of the energy for this acceleration, ultimately, is the magnetic field, though the process through which this acceleration occurs is debated by, for example, Klimchuk (2006), Scudder (1994), van Ballegoijen et al. (2014), and many others. Energy deposition by Alfvén waves and bursts of energetic particles preferentially escaping to the corona are some of the mechanisms used in models to describe this acceleration behavior (e.g., Chashei et al. 1999; Hollweg et al. 1982; and others). Our understanding of the source of the plasma acceleration has been hindered by the lack of magnetic field observations independent of the energetic properties within bursts and along closed magnetic field lines.

CMEs are unique in that they are more energetic, structured, and dominant than the regional plasma conditions. They frequently erupt with associated energetic flares, consist of an internal force-free magnetic field structure, and acquire speeds that can be 2–4 times larger than the surrounding solar wind. The magnetic fields of these structures have rarely been observed during the acceleration process between 2 and 10 solar radii (Levy et al. 1969; Bird et al. 1985; Jensen & Russell 2008). The few early observations with Helios 1 and 2 displayed large-scale force-free structure, though at the time it was not well understood. Revisiting these observations, new

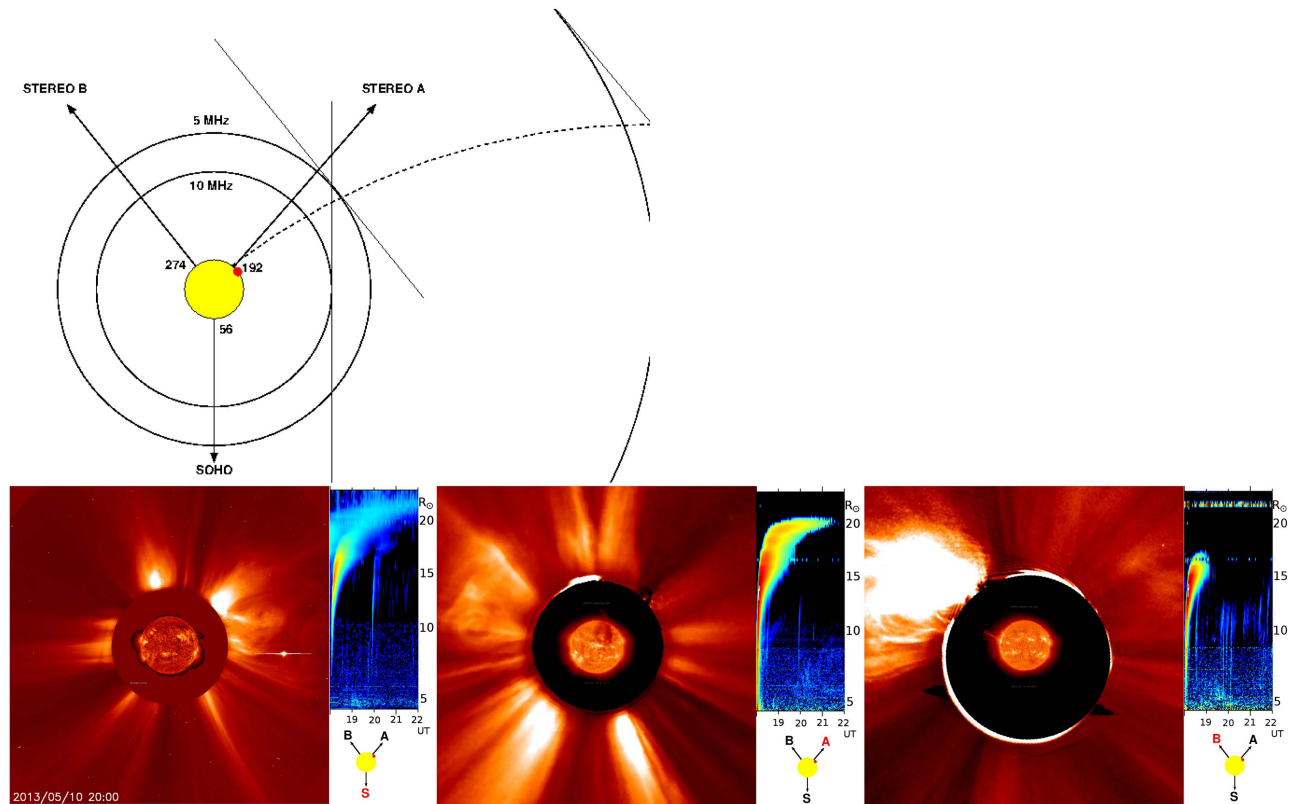


Figure 1. Top: the estimated trajectory of the CME is shown by the dashed line; the longitudinal angles for the three spacecraft are shown in solar coordinates (*SOHO* is in the direction of Earth). Bottom left panel: data from the *SOHO* and *WIND* (Earth orbiting) spacecraft. Center panel: *STEREO A*. Right panel: *STEREO B*. The radio spectrograms span 20 kHz to 15 MHz and 1800–2200 UT; their frequency axes are labeled with the solar radius for which the frequency corresponds to the local plasma frequency for an active Sun.

details have been discovered about this early phase of CME structure. These early observations showed no rotation into the force-free configuration while passing through the corona; rather, they attained the force-free configuration either before or during eruption (Jensen & Russell 2008). However, more detailed information on the magnetic field component of these CME structures could not be inferred from the available data.

New observations of a CME that occurred in 2013 were made using the *MERcury Surface, Space ENvironment, Geochemistry, and Ranging (MESSENGER)* spacecraft’s radio science and communications system. These observations were conducted in the acceleration region. Using new data processing techniques enabled the simultaneous measurement and separation of the velocity, density, and magnetic field properties of the CME structure. This is the first opportunity for a detailed examination of the models currently in use to study the acceleration region and a first look at new plasma physics relative to the CME’s evolving structure as it accelerates.

The *MESSENGER* spacecraft was in superior conjunction with its radio frequency transmissions passing through the solar corona to reach the Earth. The coronal plasma affected the signal’s intensity, phase, polarization, and frequency. The analysis of these effects allowed the simultaneous measurement of the average velocity in the plane of the sky, the change in total electron content (TEC) along the signal path, and the average magnetic field parallel to the signal path (in conjunction with a polarization brightness measurement).

On 2013 May 10, we were measuring the effects of coronal plasma on *MESSENGER* signal using the Green Bank Telescope. The *Solar and Heliospheric Observatory (SOHO)*

and the *Solar Terrestrial Relations Observatory Ahead* spacecraft (*STEREO A* and *STEREO B*) were located between 90° and 135° degrees away from each other, enabling optimal geometric viewing of a CME. Around 1800 UT, all spacecraft registered a Type III burst occurring on the western limb of the Sun. Using the frequency at which the burst became visible to the three different spacecraft, its source was restricted to two potential sunspot groups, 1728 or 1731, located at Carrington longitudes 218° and 187° . The Earth was located at 56° , and the plane-of-the-sky was at 146° . A CME from sunspot group 1728 crossing the line of sight at an offset of 72° (from the plane-of-the-sky) has too little impact on the signal due to its distance from the Sun when it crosses. Therefore, we assume that the resulting CME originated from the 1731 sunspot group at an offset of 41° from the plane-of-the-sky (Figure 1). Because CMEs can shift longitudinally as they exit the corona, we have also calculated the effect of an offset to 14° for comparison.

As shown in Figure 2 (Panel (D), insets 1–4), a CME erupted and crossed *MESSENGER*’s line of sight to Earth. The Faraday rotation (FR) signal characteristics of a CME structure have been observed before (Jensen & Russell 2008). FR is proportional to the integrated product of the electron density and the magnetic field component parallel to the signal path using the right- and left-handed components of the signal (RCP, LCP). However, eliminating the contribution from the electron density to distinguish how well the magnetic field within the structure resembled a simple force-free magnetic flux rope remained elusive in these previous observations. Additionally, any structures trailing CMEs are absent from the

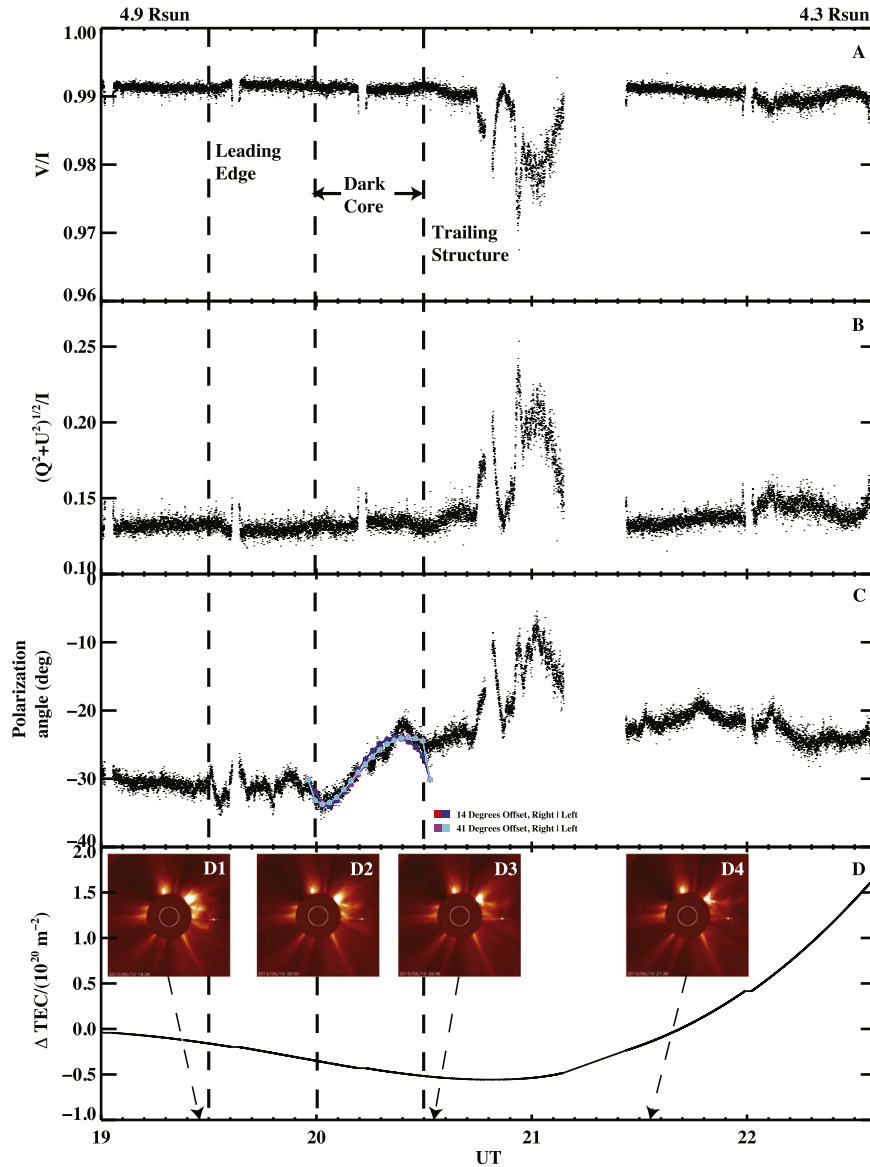


Figure 2. Panel (A): the % circular polarization of the *MESSENGER* radio frequency signal with time. Offset distances of the signal from the center of the Sun are shown at the top. Significant regions of the CME and surrounding plasma are labeled “Leading Edge,” “Dark Core,” and “Trailing Structure.” Panel (B): the % linear polarization of the *MESSENGER* signal. Panel (C): the polarization angle of the *MESSENGER* signal showing the FR. Force-free magnetic flux rope fits are overlaid in color. Panel (D): the change in TEC as determined from the technique in Jensen et al. (2016). White-light images from *SOHO* at the time periods shown are provided. *MESSENGER* was in orbit around Mercury, which is visible as a dot to the right of the disk.

literature. In the past couple of years, an engineering/scientific breakthrough was made in utilizing the same signal to measure TEC with phase rather than group velocity (Jensen et al. 2016). This allowed both the measurement of the magnetic field of the magnetic flux rope and the estimation of the average magnetic field in the trailing turbulence. The method is via the fluctuating frequency of the spacecraft’s narrow-band signal carrier. While fluctuations due to Doppler motion are dependent only on the relative motions of the spacecraft and the observer on Earth, the signal also experiences frequency fluctuations due to the changing plasma along the line of sight. The variable index of refraction induces an apparent Doppler motion of the source. The integration of these plasma fluctuations gives the *change* in TEC with time as shown in Figure 2 Panel (D). The fluctuations used in the calculation are shown in Figure 3 Panel (B).

The wave speeds of the plasma in the plane-of-the-sky are determined using the technique of Imamura et al. (2014). This is a theoretical technique developed from Kolmogorov turbulent spectral behavior of plasma by Yakovlev (2002). The frequency scintillation develops a “knee” from the characteristic turbulence scales in the plasma, and this knee gives the velocity of the turbulence. As shown in Figure 3’s Panel (C), the velocity of the CME is on average around 750 km s^{-1} ; this is the same speed that was determined from the white-light *SOHO* observations of 769 km s^{-1} .¹⁰

Figure 3’s Panel (A) exhibits the continuum system temperature Stokes I (black, combined polarized and unpolarized components), linear polarization Stokes $(Q^2 + U^2)^{1/2}$ (red), and Stokes V (green, circular polarization component).

¹⁰ SoHO LASCO CME Catalog, http://www.lmsal.com/solarsoft/www_getcme_list.html.

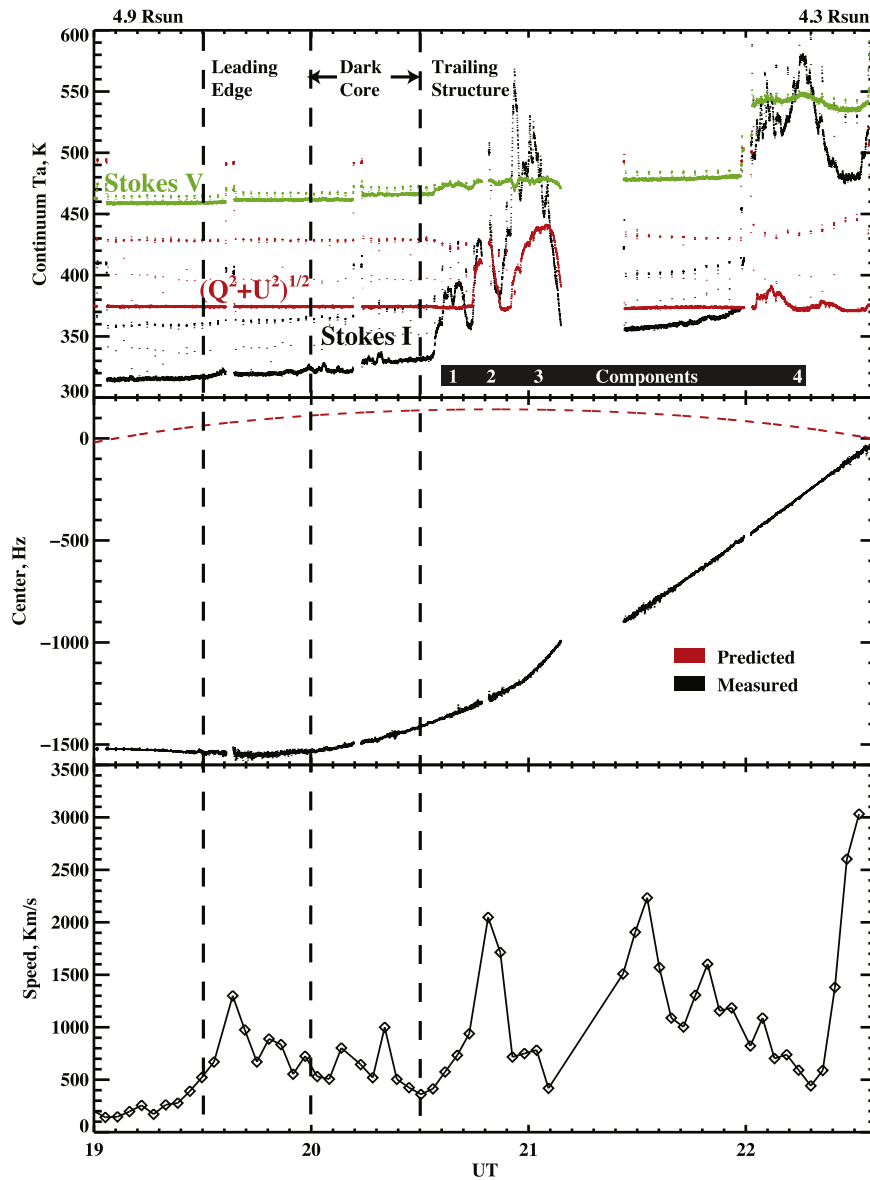


Figure 3. Panel (A): GBT System Temperature in Stokes I (black), linear polarization ($Q^2 + Y^2$) $^{1/2}$ (red), and Stokes V (green) with 4 components of enhanced temperature. We have displaced the two polarized plots by ~ 370 and 460 K. Panel (B): the predicted vs. measured Doppler frequency of the *MESSENGER* signal. Note that the difference prior to 1900 UT was a few Hz. This is the data used to measure the change in TEC shown in Figure 2 using the technique of Jensen et al. (2016). Panel (C): plasma speed across the line of sight as determined for the *MESSENGER* signal intensity spectrum using the technique of Imamura et al. (2014).

These are integrals of the spectral power over the central portion of the bandpass. The zero levels of the two polarized powers are displaced by about 370 and 460 K. Before 20.6 UT, most of the system temperature is unpolarized free-free emission from the Sun leaking into the telescope sidelobes with a level of about 350 K; after 20.6 UT there are two large enhancements. The first lasts until about 21.2 UT; it is associated with the trailing structure. Visually, it looks like it has three individual “components” in time, each producing a separate peak in the time series and lasting a few minutes. The second enhancement begins at about 22.0 UT and extends beyond our observed time range. Visual inspection shows that the components 2 and 3 of the first enhancement are about 30% linearly polarized and the second is about 75% circularly polarized.

Because of the polarization of the components, they are not simply increases in system temperature from free-free

emission. They must occur from magnetic-field-associated nonthermal processes. While the presence of cm wavelength bursts in the corona would explain the observations, none were observed. The mechanism for the bursts to cause the observed signal effects would be through the enhancement of polarized radiation in the sidelobe of the antenna (Whiting & Spangler 2009). In the absence of the burst noise mechanism, we have an alternate explanation for how this could be possible.

3. Reconnection in the Wake

The trailing turbulence shows enhanced radio noise in the beam (resonant wave mode growth), strong magnetic fields (very low electron density) peaking where the resonance is greatest, and mode conversion (Figures 2 and 3). Mode conversion is the change in the degree of linear polarization as the power in the RCP varies relative to the LCP. The

fundamental physical process occurring behind the CME in the trailing structure in our data is the cavitation from its quick passage through the acceleration region relative to the surrounding plasma; note that the TEC in Figure 2 Panel (D) reaches its minimum value between 20.6 and 21.1 UT. We show that while the downstream plasma was moving at approximately 100 km s^{-1} , the CME velocity was approximately 750 km s^{-1} . A void is created behind the CME in the trailing structure into which magnetic field lines will bend to create a force balance; this is a slow mode configuration with low electron density and high magnetic field strength. Depending on the scale size of the magnetic field fluctuations in the region relative to the perpendicular velocity of the particles, these conditions can trigger magnetic reconnection (magnetic Reynold's number around unity).

These observations open up a body of work heretofore unknown in the study of CME velocity evolution and its impact on the surrounding plasma. As the system temperature shows in Figure 3's Panel (A), local radio enhancements occurred at 4 component times immediately trailing the CME's passage. As magnetic reconnection is the most likely source of the detected signal effects, the topology of reconnection should be compared against the observations (e.g., see Mistry et al. 2015).

Ideally, two magnetic field lines with an anti-parallel component moving into a current sheet between them diffusively interact and reconfigure as two new anti-parallel magnetic field lines ejected perpendicular to the initial flow at high velocity. The change in the degree of linear polarization from mode conversion indicates that the plasma conditions are significantly different in this region. The change in the degree of linear polarization for the signal passing through the plasma in this corner of the Clemmow-Mullaly-Allis (CMA) solution space for the cold plasma is accomplished by weakening the power of the RCP transmission passed through the plasma where it nears the cutoff while the LCP power continues to transmit through relatively unaffected. However, the magnetic field measurements in Table 1 show that the necessary strength required for the gyrofrequency to reach the signal frequency cannot occur; they need to be at least three orders of magnitude larger. Therefore, we need to reexamine the wave modes for a high-frequency signal traversing a plasma with relatively low magnetic field strength and density.

Recalculating the effects on the index of refraction from the equation of motion, Faraday's Law, Ampere's Law, Poisson Equation, and the conservation of current continuity under the presence of an electric guide field from a polarization current perpendicular to the magnetic field and direction of signal propagation, we find that the FR RCP and LCP wave equations are modified (see the Appendix):

$$\left\{ \begin{array}{l} R n_c^2 = 1 - \frac{\omega_{pe}^2/\omega^2}{\left(1 - \frac{\Omega_{ce}}{\omega}\right)} \\ L n_c^2 = \left(1 - \frac{\omega_{pe}^2/\omega^2}{\left(1 + \frac{\Omega_{ce}}{\omega}\right)}\right), \left(1 + i \left(1 - \frac{\omega_{pe}^2/\omega^2}{\left(1 + \frac{\Omega_{ce}}{\omega} \eta\right)}\right)\right) \end{array} \right\}, \quad (1)$$

where n_c is the index of refraction, ω_{pe} is the plasma frequency, ω is the signal frequency, Ω_{ce} is the electron cyclotron frequency, Ω_{ci} is the ion cyclotron frequency, ω_g is the frequency for electric guide field fluctuations, and η is the

modifying factor in the imaginary component as follows:

$$\eta = \frac{\frac{w_g \Omega_{ce}}{\omega_{pe}^2}}{1 - \frac{\omega \omega_g}{\Omega_{ce} \Omega_{ci}} - \frac{\omega \omega_g}{\Omega_{ce}^2} - \frac{\omega \omega_g}{\omega_{pe}^2}}. \quad (2)$$

The first wave mode is the familiar FR solution. The second for LCP includes an imaginary component created by the electric guide field. A positive imaginary dispersion relation component gives rise to wave growth. Under coronal conditions, the fraction subtracted from 1 in the imaginary wave mode is around 5×10^{-5} ; this is a similar magnitude as the fraction subtracted from 1 for the FR solution.

The mode conversion seen in the data indicates that the phenomenon is increasing the measured system temperature via increasing the energy of the propagating LCP wave modes. For a parallel magnetic field, the RCP corresponds to the direction of rotation of electrons around the magnetic field line; the LCP is moving against the electron gyromotion, so it has a slower phase speed.

It is worth mentioning that this trailing structure alone in FR data that could be caused by reconnection is easy to misidentify as another magnetic flux rope. Following this data collection and analysis, it appears that the *Pioneer 6* transients in Jensen & Russell (2008) were possibly similar reconnection structures (consisting of similar shapes in reversed direction); unfortunately, that data set did not include the measurement of the degree of linear polarization of the signal in order to verify this interpretation.

Shortly before the observation ended, another region of enhanced system temperature was observed and measured (Figure 3, Component 4). Unlike the plasma trailing the CME, this is in a plasma environment where the density is enhanced and the parallel magnetic field and degrees of polarization are relatively unaffected. As can be seen in the white-light images for the time, 2200 UT occurs after the line of sight has crossed into an enhanced density streamer region and is likely associated with a current sheet, as can be seen by the minor increase and decrease in parallel magnetic field strength relative to the enhanced temperature peaks. This is another region worth studying by modifying the technique above for different signal, magnetic field, and electric field orientations.

Finally, the first component, in contrast to the following two components, shows little change in magnetic field or degree of polarization. This similarly suggests that the equations for other configurations between the signal, magnetic field, and local electric field should be calculated. Note that the plasma speed enhancements around 2130 and 2230 UT should be included when considering the plasma environment.

4. Models

Models for simulating the properties of CMEs within the acceleration region are available from the Community Coordinated Modeling Center (CCMC). Among these models the most widely used are the Wang-Sheeley-Arge-ENLIL (WSA-ENLIL) and the Gibson-Low (GL) flux rope CME models (Gibson & Low 1998; Odstrcil & Pizzo 1999). WSA-ENLIL, utilized by NOAA's Space Weather Prediction Center, initializes its MHD simulation with observations of the photosphere accompanied by an empirical formula for magnetic field and velocity. A CME is included in the model by manually fitting a cone to polarized brightness data. The GL

model inserts a 3D magnetic flux rope into the Alfvén Wave Solar Atmosphere MHD model allowing for the user-specified initial conditions to spontaneously erupt. The gradual acceleration of slow CMEs is not captured, while the deceleration of fast CMEs occurs as the triggering force imbalance relaxes. These are two specific examples of composite models, and the components within them are switched out in other varieties that can be found at the CCMC. What they have in common is that the magnetic field within the CME as it passes through the acceleration region is not compared to any existing data set. In common between all the models is that the heating, the largest energetics, and the greatest instabilities are on the leading edge where it is plowing into the surrounding, ambient solar wind plasma.

In contrast to these model results, our observations indicate that within the acceleration region the greatest activity occurs, following the trailing edge of the CME. None of the currently available MHD models indicate that there should be any activity other than the relaxation of the plasma in the trailing edge, such as the changing plasma beta, and local reconnection to balance an unstable pressure gradient; these are properties detected in our observations that cannot be modeled with MHD due to the relevant scale sizes. As we show, the models actually cannot describe this activity because it occurs on scale sizes smaller than the modeling grid. A one-degree (the finest scale) grid is around 50 Mm at 4 solar radii; in contrast, the Fresnel zone at which *MESSENGER*'s 8.4 GHz radio signal is sensitive is around 40 km. While the ENLIL cone model does not concern itself with having a flux rope magnetic field topology, its focus on the sterradian versus radial expansion is not significant within the acceleration region. Additionally, the cone model does not concern itself with the magnetic field within the flux rope, merely fitting the density enhancement that's found in the polarized brightness images. As our data show, as well as that of other researchers, the location within the CME of the magnetic flux rope is in a region of lower density. The ENLIL cone model will not reproduce the observed FR well. The GL flux rope model, in contrast, is a more advanced form than a force-free Bessel function, and we find that the simple Bessel function works well in fitting the dark core of the CME in our data occurring between 19.8 and 20.5 UT (Figure 2 polarization angle overlay, Table 1).

4.1. Discoveries

The FR characteristics trailing the CME from 20.75 to 21.25 UT cannot be explained by any of the CME models. As we discussed previously regarding the *Pioneer 6* transients, the FR signatures associated with the enhanced system temperature could be incorrectly modeled with two more CMEs if no other data exists showing that these events are not under normal plasma conditions (based on the change in the degree of linear polarization); however, they would not have the correct characteristics, namely localized increased radio brightness and sufficient magnetic field strength to impact the fractional polarization (see Figure 2). As we discussed earlier, the system temperature increase, lack of enhanced density, the enhanced plasma speeds, organized magnetic field configuration, and the associated effects on the plasma wave modes are all characteristic of reconnection. Reconnection is the process through which the plasma conditions go from being flow (MHD) dominated to diffusion dominated, where the perpendicular flow velocity vies with the scale size of the magnetic

field variations. None of the CCMC models currently capture this process; instead, they calculate across the regions where it occurs to include its ideal after-effects for magnetic field orientation, velocity, and density. The behavior on the trailing side of the CME within the acceleration region has never been previously identified in observations and therefore is not included in the modeling.

At the time of Jensen & Russell (2008), the fact that CMEs had magnetic flux rope configurations was known, allowing the straightforward calculation of their FR signatures under a variety of conditions. The calculations of FR assumed that electron density was constant. Separating the electron density contribution from the magnetic field continued to remain an open question. This work is the first to solve the deconvolution and show that the simplest force-free model works well in fitting the magnetic flux rope portion of CMEs that pass through the acceleration region. While we expect that the GL model can perform a tighter fit of the CME's dark core's magnetic flux rope, it cannot reproduce other characteristics relevant to the CME, namely the fluctuations in magnetic field that precede and follow its passage across the line of sight between the spacecraft and the Earth. The ENLIL model represents a CME as density enhancement, the reverse of which is seen in our observations, and is thus not useful for modeling the acceleration region and comparing it to this data set. The grid size on both models is too large to detect the fluctuations seen, and particularly in the case of the regions we have identified as diffusive, the MHD approximation utilized by both fails.

More important is the discovery of local, ≈ 100 km in size, regions of enhanced radio brightness (detected via system temperature) associated with changes in signal polarization. As changes in the degree of linear polarization require mode conversion, the possible solutions for the observations become increasingly limited to the phenomenon of magnetic reconnection or as yet undetected cm bursts in the corona. These are the first observations of the phenomena trailing a CME's passage through the acceleration region of the solar corona. The acceleration region is a critical area of evolution for the solar wind and CMEs as they change velocity (increasing/decreasing if the initial CME speed is relatively slow/fast). Its dominant properties of density, velocity, and magnetic field are rarely simultaneously measured, leaving space weather research dependent on untested models for the region. This is the first data set obtained for a CME passage at a 40 km scale size and 1 s resolution.

Solar wind interactions with planetary bodies greatly depend on the presence of an atmosphere and/or magnetic field. Both restrict the majority of the interaction to the magnetized plasma (intrinsic or inductive) above the body's surface. Examples include comets (atmosphere with inductive magnetization) and Mercury (magnetosphere with intrinsic magnetization). Bodies such as asteroids and the moon are exposed directly to the impinging solar plasma. All of these interactions are studied with models for the solar contribution. This work is critical for determining limits to time-variable solar plasma phenomena and learning at what scales in space and time that plasma interactions from these phenomena have a lasting effect. Does an icy asteroid such as Ceres carry a record of extreme solar events in its frozen surface? Does the moon have such a record in the crystal grains below its regolith?

Table 1
Magnetic Force-free Flux Rope Fits to Data Using the Technique from Jensen & Russell (2008)

Hand	Offset (°)	$N (\times 10^{11} \text{ m}^{-3})$	Axial B (nT)	Xing (Rs)	Size (Rs)	Clock (°)	Cone (°)
Left	41	2.58	2.7	6.3	1.1	271	76
Right	41	2.58	2.9	6.3	1.0	94	75
Right	41	1.98	3.8	6.3	1.0	95	75
Left	41	1.98	3.5	6.3	1.1	271	76
Left	41	2.36	2.9	6.3	1.1	271	76
Right	41	2.36	3.2	6.3	1.0	94	75
Right	14	7.82	1.2	4.9	0.9	88	78
Left	14	7.82	1.3	4.9	0.9	266	79
Left	14	6.00	1.6	4.9	0.9	266	79
Right	14	6.00	1.6	4.9	0.9	88	78
Right	14	7.15	1.3	4.9	0.9	88	78
Left	14	7.15	1.3	4.9	0.9	266	79

Note. Offset is the angle of CME travel relative to the sun–line-of-sight point of closest approach, Xing is the radial distance of the CME from the Sun when it is crossing the line of sight, and the cone and clock angles are relative to the line of sight, with the clock angle in the plane of the sky and the cone angle being the colatitude of the coordinate system off of the line-of-sight axis. The clock angle axes are radial at the point of closest approach, and perpendicular to the line of sight and this axis, for completing the right-handed coordinate system. Within the context of the relative positions of Earth, the Sun, and *MESSENGER* during these observations, a 90° clock and cone angle are roughly in the direction normal to the ecliptic plane.

Other questions are raised by these observations on the evolution of the solar wind itself before impacting exposed surfaces. Does the reconnection trailing a CME play a role in its evolution? Does it stop? Is it aperiodic, dependent on the downstream plasma properties?

These data observations need to be simulated in the lab, more observations need to be collected, and models need to be modified to properly understand the physics taking place. CMEs are significant in solar wind dynamics and how the plasma interacts with other objects in interplanetary space. The *Solar Probe Plus* mission, soon to be launched to obtain in situ CME measurements down to 10 Rs, will enable confirmation of this theory of reconnection regions trailing CMEs.

5. Conclusions

On 2013 May 10, a CME crossed the line of sight between the *MESSENGER* spacecraft orbiting Mercury and the Earth. The CME’s structure was composed of three distinct features: (1) from 19.5 to 20UT, the columnar density decreases slowly while the signal tone’s frequency width increases with increasing speeds from 100 to 500 km s⁻¹; (2) from 20 to 20.5 UT, the columnar density decreases faster as the signal width decreases to a local minimum during the sigmoidal rotation in polarization angle with speeds around 750 km s⁻¹; and (3) from 20.5 to 21 UT columnar densities are at their lowest, speeds are variable between 500 and 1000 km s⁻¹, the polarization angle experiences strong rotations accompanied by strong changes in the degree of circular polarization, and the system temperature is variable.

After the CME’s passage, the density recovers rapidly and continues to increase, the speed decreases from around 1500 to 500 km s⁻¹ and the system temperature is variable (from 22 to 22.5 UT). The behavior in the structure (2), the dark core, is the well modeled and understood magnetic flux rope. The behavior trailing the CME’s passage has not been observed before. Its characteristics are unique, particularly the change in the degree of linear polarization, such that only two explanations are available: plasma mode conversion as a result of reconnection, and cm wavelength bursts on the Sun impacting the measurement via the antenna’s sidelobe (not observed). These observations suggest that space weather research and storm

prediction should include the trailing characteristics of a CME impact, as well as its initial ram pressure and magnetic flux rope configuration.

The authors thank Timothy Howard, who processed the white-light images, enabling estimates of the magnetic field strength. We also thank Amanda Hendrix, Jean-Luc Margot, Karen O’Neil, Mark Perry, the *MESSENGER* spacecraft team, and NRAO’s Green Bank Telescope team. This research was supported by the *MESSENGER* Participating Scientist program, NASA Contracts NNX07AT38G and NASW-00002, and ACS Consulting, LLC. This work was performed in part at the Jet Propulsion Laboratory, California Institute of Technology under contract with the National Aeronautics and Space Administration.

Facilities: NRAO/GBT, *SOHO*.

Appendix Plasma Calculations for the Effect of an Electric Guide Field on EM Wave Propagation

A plasma structure trailing a CME was measured at the same time the signal’s degree of polarization increased, as well as the signal’s polarized intensity. Assuming the process of reconnection was occurring to affect the signal, we calculate the plasma dispersion relations necessary to reproduce the observed signal effects.

A.1. Introduction

On 2013 May 10, the *MESSENGER* spacecraft was in superior conjunction. This unique configuration with the solar corona in the path of the spacecraft’s radio frequency signal to the Earth enabled the remote measurement of a CME that erupted and crossed the signal path. The analysis of the degree of polarization of the signal showed significant changes within the TRAILING structure following the CME’s passage.

The two possibilities for the increase in linear polarization are (a) a radio frequency burst of cyclotron radiation and (b) an unknown wave propagation mode preferentially affecting the left-handed component of a traversing electromagnetic wave. We cannot analyze (a) because no detectable bursts were

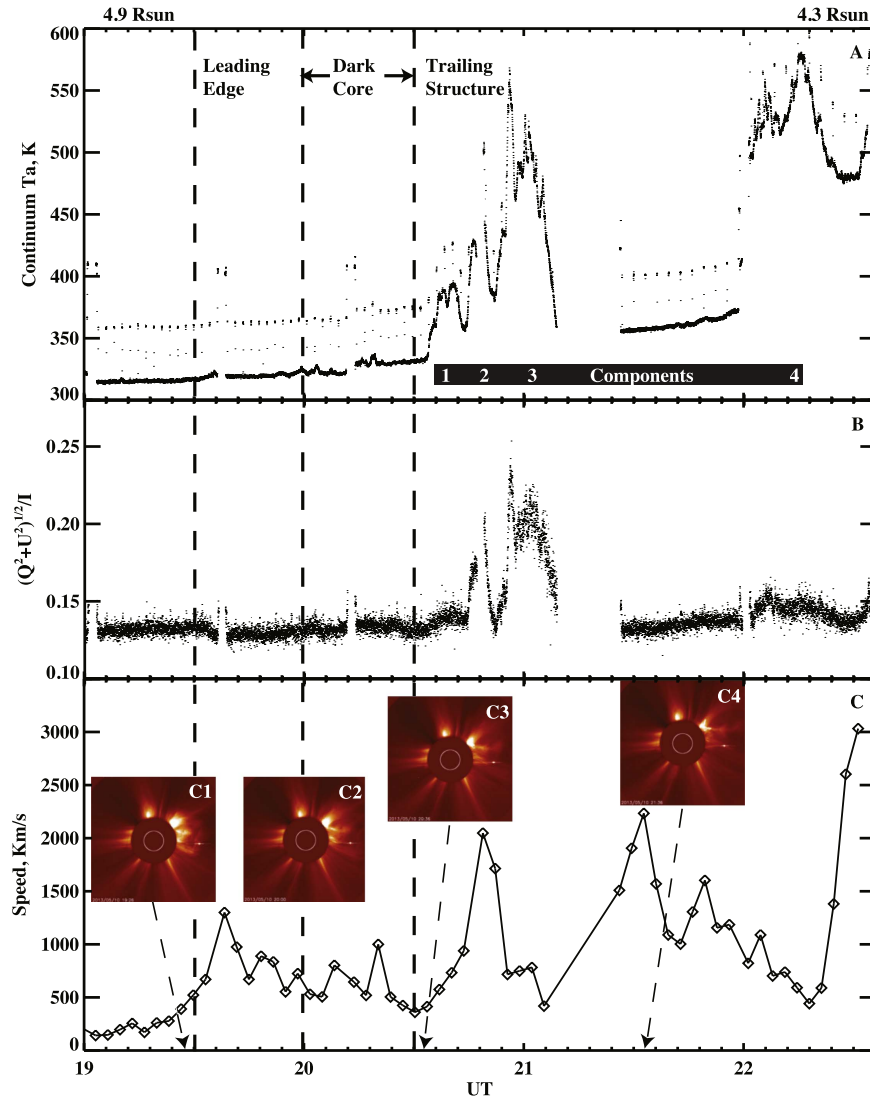


Figure 4. Panel (A): GBT System Temperature with 4 components of enhanced temperature. Panel (B): the % linear polarization of the *MESSENGER* signal. Panel (C): plasma speed across the line of sight as determined of the *MESSENGER* signal intensity spectrum. White-light images from *SOHO* at the time periods shown are provided. *MESSENGER* was in orbit around Mercury, which is visible to the right of the disk. See Figures 2 and 3 for more details.

observed that could correspond with the signal fluctuations. Assuming (b) was the case, meaning the change in the degree of linear polarization was due to unusual plasma conditions in the trailing structure, we set about to investigate what a possible solution could be.

A.2. Reconnection in the Wake

The trailing turbulence shows enhanced radio noise in the beam (resonant wave mode growth), strong magnetic fields (very low electron density) peaking where the resonance is greatest, and mode conversion (Figure 4). Mode conversion is the change in the degree of linear polarization as the power in the RCP varies relative to the LCP. The fundamental physical process occurring behind the CME in the trailing structure is the cavitation from its quick passage (1000 km s^{-1}) through the surrounding plasma (100 km s^{-1} , Panel (C)). A void is created behind the CME comprising the trailing structure into which magnetic field lines will bend to create a force balance; this is a slow mode configuration with low electron density and high magnetic field strength. Depending on the scale size of the

magnetic field fluctuations in the region relative to the perpendicular velocity of the particles, these conditions can trigger magnetic reconnection (magnetic Reynold's number around unity).

The change in the degree of linear polarization from mode conversion indicates that the plasma conditions are significantly different in this region. Under cold plasma conditions for mode conversion to occur, the magnetic field would have to be significantly stronger such that its gyrofrequency approaches the signal frequency in order to begin preferentially absorbing/reflecting the RCP power until it is completely lost at the RCP cutoff. The change in the degree of linear polarization for the signal passing through the plasma in this corner of the CMA solution space for the cold plasma is accomplished by weakening the power of the RCP transmission passed through the plasma where it nears the cutoff, while the LCP power continues to transmit despite being relatively unaffected. However, the magnetic field measurements show that the necessary strength required for the gyrofrequency to reach the signal frequency cannot occur. Therefore, we need to reexamine the wave modes for a high-frequency signal

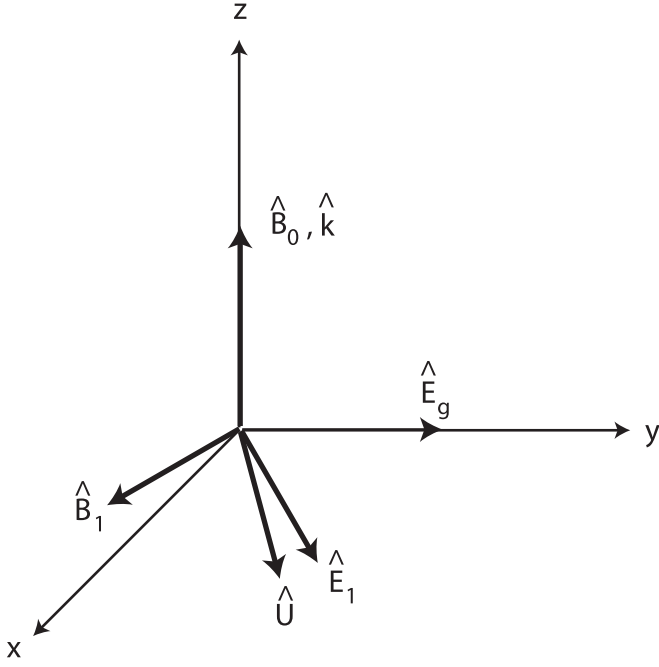


Figure 5. Vector orientations for the calculations of the system of equations in this paper. E is the electric field (guide and perturbed), B is the magnetic field (background and perturbed), U is the velocity of the perturbation, and k is the propagation direction of the traversing wave.

traversing a plasma with relatively low magnetic field strength and density (Kivelson & Russell 1995).

Magnetic reconnection comprises unusual plasma conditions, making it the most likely source of the detected signal effects. The topology of reconnection (e.g., see Mistry et al. 2015) is modeled with two magnetic field lines with an anti-parallel component moving into a current sheet between them. They diffusively interact and get reconfigured as two new anti-parallel magnetic field lines ejected perpendicular to the initial flow. An electric guide field plays a critical role in this process.

A.3. Equation Setup

Recalculating the effects on the index of refraction from the Equation of Motion, Faraday's Law, Ampere's Law, Poisson Equation, and Current Continuity under the presence of an electric guide field from a polarization current perpendicular to the magnetic field and direction of signal propagation, we find the following for the configuration shown in Figure 5:

equation of motion

$$\left\{ \begin{array}{l} 0 = m_e n_o \frac{du_1}{dt} + en_o E_1 + en_o E_g \\ \quad + \mathbf{j} \times \mathbf{B} \\ \mathbf{j} = en_o \mathbf{u}_1 - \frac{n_o(m_i + m_e)}{B^2} \frac{dE_g}{dt} \end{array} \right\} \quad (3)$$

where $m_{e,i}$ is the mass of an electron/ion, u_1 is the perpendicular velocity of the wave, e is the electron charge, E_1 is the perpendicular electric field of the wave, n_o is the density of electrons/ions, E_g is the electric guide field of the reconnection region, and B is the background magnetic field.

Assuming that for the time in which the signal is traversing the structure, its guide field spatial variations are not centimeter-scale like the signal's wavelength, then Faraday's

Law is expressed as

$$\left\{ \begin{array}{l} 0 = \nabla \times \mathbf{E}_1 + \frac{d\mathbf{B}_1}{dt} \\ 0 = \nabla \times \mathbf{E}_g \end{array} \right\}; \quad (4)$$

Ampere's Law is

$$\left\{ \begin{array}{l} \nabla \times \mathbf{B}_1 = -en_o \mathbf{u}_1 + \mu \mathbf{j} \\ \quad + \frac{1}{c^2} \frac{dE_1}{dt} + \frac{1}{c^2} \frac{dE_g}{dt} \end{array} \right\}; \quad (5)$$

where B_1 is the perpendicular magnetic field of the wave, and μ is the magnetic permeability of free space. These become

equation of motion

$$\left\{ \begin{array}{l} \hat{x} \ m_e n_o \frac{du_x}{dt} + en_o E_{1x} + en_o u_y B - \frac{n_o(m_i + m_e)}{B^2} \frac{dE_{gy}}{dt} B = 0 \\ \hat{y} \ m_e n_o \frac{du_y}{dt} + en_o E_{1y} + en_o E_{gy} - en_o u_x B = 0 \\ \hat{z} \ 0 = 0 \end{array} \right\}; \quad (6)$$

Faraday's Law

$$\left\{ \begin{array}{l} \hat{x} \ -\frac{dB_{1y}}{dz} + \frac{dB_{1x}}{dt} = 0 \\ \hat{y} \ \frac{dE_{1x}}{dz} + \frac{dB_{1y}}{dt} = 0 \\ \hat{z} \ 0 = 0 \end{array} \right\}; \quad (7)$$

and Ampere's Law

$$\left\{ \begin{array}{l} \hat{x} \ -\frac{dB_{1y}}{dz} = -\mu en_o u_x + \frac{1}{c^2} \frac{dE_{1x}}{dt} \\ \hat{y} \ \frac{dB_{1x}}{dz} = -\mu en_o u_y + \mu \frac{n_o(m_i + m_e)}{B^2} \frac{dE_{gy}}{dt} + \frac{1}{c^2} \frac{dE_{1y}}{dt} + \frac{1}{c^2} \frac{dE_{gy}}{dt} \\ \hat{z} \ 0 = 0 \end{array} \right\}. \quad (8)$$

These become

equation of motion

$$\left\{ \begin{array}{l} \hat{x} \ -i\omega m_e n_o u_x + en_o E_{1x} + en_o u_y B_o + \frac{i\omega_g}{B_o} n_o(m_i + m_e) E_g = 0 \\ \hat{y} \ -i\omega m_e n_o u_y + en_o E_{1y} + en_o E_g - en_o u_x B_o = 0 \\ \hat{z} \ 0 = 0 \end{array} \right\}, \quad (9)$$

where ω is the signal frequency and ω_g is the frequency of the guide field.

Faraday's Law is

$$\left\{ \begin{array}{l} \hat{x} \ kE_{1y} = -\omega B_{1x} \\ \hat{y} \ kE_{1x} = \omega B_{1y} \\ \hat{z} \ 0 = 0 \end{array} \right\}, \quad (10)$$

where k is the signal wavenumber.

Ampere's Law is

$$\left\{ \begin{array}{l} \hat{x} \ ikB_{1y} = \mu en_o u_x + \frac{i\omega}{c^2} E_{1x} \\ \hat{y} \ ikB_{1x} = -\mu en_o u_y - i\omega_g \mu n_o(m_i + m_e) \frac{E_g}{B^2} - \frac{i\omega}{c^2} E_{1y} - \frac{i\omega_g}{c^2} E_g \\ \hat{z} \ 0 = 0 \end{array} \right\}. \quad (11)$$

Substituting the Faraday's solutions into the Ampere's Law dispersion equations gives

$$\left\{ \begin{array}{l} \hat{x} \quad ik \frac{kE_{1x}}{\omega} = \mu en_o u_x + \frac{i\omega}{c^2} E_{1x} \\ \hat{y} \quad -ik \frac{kE_{1y}}{\omega} = -\mu en_o u_y - i\omega_g \mu n_o (m_i + m_e) \frac{E_g}{B^2} - \frac{i\omega}{c^2} E_{1y} - \frac{i\omega_g}{c^2} E_g \\ \hat{z} \quad 0 = 0 \end{array} \right\} \quad (12)$$

This gives the following solutions for the wave speed:

$$\left\{ \begin{array}{l} \hat{x} \quad u_x = -\frac{i\epsilon\omega}{en_o} \left(1 - \frac{k^2 c^2}{\omega^2}\right) E_{1x} \\ \hat{y} \quad u_y = -\frac{i\epsilon}{\omega en_o} (-k^2 c^2 + \omega^2) E_{1y} - \frac{i\omega_g}{e} \left(\frac{m_i + m_e}{B^2} + \frac{\epsilon}{n_o}\right) E_g \end{array} \right\} \quad (13)$$

where ϵ is the permittivity of free space.

Now we take these solutions and put them back into the Equation of Motion dispersion equation. After some algebra, this becomes

$$\left\{ \begin{array}{l} \hat{x} \quad E_{1x} \left(en_o - \frac{m_e \epsilon}{e} (\omega^2 - k^2 c^2)\right) - iE_{1y} \left(\frac{B\epsilon}{\omega} (\omega^2 - k^2 c^2)\right) - iE_g (\omega_g B\epsilon) = 0 \\ \hat{y} \quad iE_{1x} \left(\frac{B\epsilon}{\omega} (\omega^2 - k^2 c^2)\right) + E_{1y} \left(en_o - \frac{m_e \epsilon}{e} (\omega^2 - k^2 c^2)\right) \\ \quad + E_g \left(en_o - \frac{m_e \omega \omega_g}{B^2 e} (n_o m_i + n_o m_e + B^2 \epsilon)\right) = 0 \\ \hat{z} \quad 0 = 0 \end{array} \right\} \quad (14)$$

Definitions are as follows:

$$\left\{ \begin{array}{l} \gamma = \omega^2 - k^2 c^2 \\ \omega_{pe}^2 = \frac{e^2 n_o}{m_e \epsilon} \\ \Omega_{ce,i}^2 = \frac{B^2 e^2}{m_{e,i}} \end{array} \right\} \quad (15)$$

where ω_{pe} is the plasma frequency, Ω_{ce} is the electron cyclotron frequency, and Ω_{ci} is the ion cyclotron frequency.

Then, we can express the equations as

$$\left\{ \begin{array}{l} 0 = E_{1x} \left(1 - \frac{\gamma}{\omega_{pe}^2}\right) - iE_{1y} \left(\frac{\Omega_{ce}\gamma}{\omega\omega_{pe}^2}\right) - iE_g \left(\frac{\omega_g \Omega_{ce}}{\omega_{pe}^2}\right) \\ 0 = iE_{1x} \left(\frac{\Omega_{ce}\gamma}{\omega\omega_{pe}^2}\right) + E_{1y} \left(1 - \frac{\gamma}{\omega_{pe}^2}\right) + E_g \left(1 - \frac{\omega\omega_g}{\Omega_{ce}\Omega_{ci}} - \frac{\omega\omega_g}{\Omega_{ce}^2} - \frac{\omega\omega_g}{\omega_{pe}^2}\right) \end{array} \right\} \quad (16)$$

which is two equations and three unknowns. Since we are introducing a guide field, the Poisson and the current continuity equations become important.

Poisson's equation is:

$$\left\{ \nabla \cdot \mathbf{E} = \frac{\rho_q}{\epsilon} \right\} \quad (17)$$

The current continuity equation is

$$\left\{ \frac{d\rho_q}{dt} + \nabla \cdot \mathbf{j} = 0 \right\} \quad (18)$$

Combining these together, along with the change in charge density with time, gives

$$\left\{ \epsilon \frac{d}{dt} (\nabla \cdot \mathbf{E}) = -\nabla \cdot \mathbf{j} \right\} \quad (19)$$

Assuming the partial derivatives are commutative, the equation can be rewritten as

$$\left\{ \epsilon \frac{d\mathbf{E}}{dt} = -\mathbf{j} \right\} \quad (20)$$

In Cartesian coordinates, this becomes

$$\left\{ \begin{array}{l} \hat{x} \quad \epsilon (-i\omega) E_{1x} = -(-en_o u_{1x}) \\ \hat{y} \quad i\epsilon (\omega E_{1y} + \omega_g E_g) = -en_o u_{1y} + \frac{n_o (m_i + m_e)}{B^2} \frac{dE_g}{dt} \end{array} \right\} \quad (21)$$

Substituting the solutions for $u_{1x,1y}$, this becomes

$$\left\{ \begin{array}{l} \hat{x} \quad 0 = E_{1x} i \frac{k^2 c^2}{\omega^2} \\ \hat{y} \quad 0 = E_{1y} i \left(1 - \frac{\gamma}{\omega^2}\right) \end{array} \right\} \quad (22)$$

So combining all these together gives

$$\left\{ \begin{array}{l} \left(1 - \frac{\gamma}{\omega_{pe}^2}\right) \quad -i \left(\frac{\Omega_{ce}\gamma}{\omega\omega_{pe}^2}\right) \quad -i \left(\frac{\omega_g \Omega_{ce}}{\omega_{pe}^2}\right) \\ i \left(\frac{\Omega_{ce}\gamma}{\omega\omega_{pe}^2}\right) \quad \left(1 - \frac{\gamma}{\omega_{pe}^2}\right) \quad \left(1 - \frac{\omega\omega_g}{\Omega_{ce}\Omega_{ci}} - \frac{\omega\omega_g}{\Omega_{ce}^2} - \frac{\omega\omega_g}{\omega_{pe}^2}\right) \\ i \frac{k^2 c^2}{\omega^2} \quad i \left(1 - \frac{\gamma}{\omega^2}\right) \quad 0 \end{array} \right\} \times \left\{ \begin{array}{l} E_{1x} \\ E_{1y} \\ E_g \end{array} \right\} \quad (23)$$

If we set the following variables

$$\left\{ \begin{array}{l} A = 1 - \frac{\gamma}{\omega_{pe}^2} \\ C = \frac{\Omega_{ce}\gamma}{\omega\omega_{pe}^2} \\ D = \frac{\omega_g \Omega_{ce}}{\omega_{pe}^2} \\ E = 1 - \frac{\omega\omega_g}{\Omega_{ce}\Omega_{ci}} - \frac{\omega\omega_g}{\Omega_{ce}^2} - \frac{\omega\omega_g}{\omega_{pe}^2} \\ F = \frac{k^2 c^2}{\omega^2} \\ G = \left(1 - \frac{\gamma}{\omega^2}\right) \end{array} \right\} \quad (24)$$

We get the following:

$$A(-iGE) + iC(-iEF) - iD(-CG - iAF) = 0. \quad (25)$$

This gives the real and imaginary solutions

$$\begin{cases} \Re & CE - AD = 0 \\ \Im & CD - AE = 0 \end{cases}. \quad (26)$$

Note that the Faraday rotation solution is found when eliminating E_g and assume the current is zero:

$$A^2 - C^2 = 0. \quad (27)$$

Now solve for the index of refraction $n_c^2 = \frac{k^2 c^2}{\omega^2}$:

$$\begin{cases} \Re & n_c^2 = 1 - \frac{\omega_{pe}^2/\omega^2}{\left(1 + \frac{\Omega_{ce} E}{\omega D}\right)} \\ \Im & n_c^2 = 1 - \frac{\omega_{pe}^2/\omega^2}{\left(1 + \frac{\Omega_{ce} D}{\omega E}\right)} \end{cases}. \quad (28)$$

Both of these solutions are left-handed, as we can see from the index of refraction for the Faraday rotation solution

$$\left\{ R, L \quad n_c^2 = 1 - \frac{\omega_{pe}^2/\omega^2}{\left(1 \mp \frac{\Omega_{ce}}{\omega}\right)} \right\}. \quad (29)$$

The real component is ≈ 1 because the ratio is on the order of 10^{-19} for solar coronal conditions. The imaginary component is slightly less than 1 by 10^{-5} . This is the same order by which Faraday rotation begins to affect the signal's phase angle. Solar coronal conditions are

$$\left. \begin{array}{l} B(T) \quad 1 \times 10^{-9} \\ \epsilon \left(\frac{s^4 A^2}{m^3 kg} \right) \quad 8.85 \times 10^{-12} \\ e(C) \quad 1.6 \times 10^{-19} \\ n(m^{-3}) \quad 1 \times 10^{12} \\ m_e(kg) \quad 9.11 \times 10^{-31} \\ m_i(kg) \quad 1.67 \times 10^{-27} \\ \omega(Hz) \quad 8 \times 10^9 \\ \omega_{pe}(Hz) \quad \sqrt{\frac{ne^2}{m_e \epsilon}} \\ \Omega_{ce,i}(Hz) \quad \frac{eB}{m_{e,i}} \\ \omega_g(Hz) \quad 10^6 \rightarrow 10^8 \end{array} \right\}. \quad (30)$$

So our final equations for the index of refraction of the right- and left-handed signals passing through a plasma with a guide field perpendicular to the magnetic field become

$$\left\{ \begin{array}{l} R \quad n_c^2 = 1 - \frac{\omega_{pe}^2/\omega^2}{\left(1 - \frac{\Omega_{ce}}{\omega}\right)} \\ L \quad n_c^2 = \left(1 - \frac{\omega_{pe}^2/\omega^2}{\left(1 + \frac{\Omega_{ce}}{\omega}\right)}\right), \left(1 + i \left(1 - \frac{\omega_{pe}^2/\omega^2}{\left(1 + \frac{\Omega_{ce} D}{\omega E}\right)}\right)\right) \end{array} \right\}. \quad (31)$$

A.4. Discussion

Equation (31) shows the two circularly polarized wave modes that are calculated to propagate through the structure trailing the CME given the vector configuration in Figure 5. The first mode in the left circular polarization is the familiar Faraday rotation solution; the second wave mode is the special one that has been calculated herein. An electromagnetic wave with the frequency of *MESSENGER*'s signal would experience left circular polarization growth because of the imaginary component of the index of refraction that is produced by the

presence of the guide field. A positive imaginary component gives rise to wave growth. Under coronal conditions, the fraction subtracted from 1 in the imaginary wave mode is around 5×10^{-5} ; this is a similar magnitude as the fraction subtracted from 1 for the Faraday rotation solution.

The mode conversion seen in the data indicates that the phenomenon is increasing the measured system temperature via increasing the polarized energy. While a burst in the corona transmitting polarized radiation into the sidelobes could achieve this effect (not observed), the calculation above indicates that a reconnection region could as well through an increase of the energy of the propagating LCP wave mode.



It is worth mentioning that this trailing structure alone in Faraday rotation data that we can associate with reconnection or unobserved burst activity is easy to misidentify as another magnetic flux rope. Following this data collection and analysis, it appears that the *Pioneer 6* transients in Jensen & Russell (2008) were possibly similar structures (consisting of similar shape); unfortunately, that data set did not include the measurement of the degree of linear polarization of the signal in order to verify this interpretation.

While the calculations above are for a single set of conditions, it's worthwhile to modify the calculations for other orientations and variabilities.

A.5. Summary

We have demonstrated that the observations shown in Figure 4 could be generated through the presence of an electric guide field. The *MESSENGER* radio frequency signal properties are capable of probing the critical, yet local and intermittent, phenomena of magnetic reconnection in the outer reaches of the solar corona, the acceleration region. Reconnection plays a significant role in solar wind evolution and dynamics, and remotely measuring the phenomenon is an important achievement. The trailing structure has stronger magnetic fields than the CME itself, and these regions of the strong fields occur over a longer period of time than the flux rope within the CME itself. This work suggests that the impact of reconnection in the trailing structure of the CME should be investigated further with regard to CME interactions with other bodies.

ORCID iDs

Elizabeth A. Jensen  <https://orcid.org/0000-0003-0216-6621>
 Carl Heiles  <https://orcid.org/0000-0002-7456-8067>
 David Wexler  <https://orcid.org/0000-0002-5763-6267>
 Amanda A. Kepley  <https://orcid.org/0000-0002-3227-4917>
 Thomas Kuiper  <https://orcid.org/0000-0003-1798-4918>
 Mario M. Bisi  <https://orcid.org/0000-0001-6821-9576>
 Deborah Domingue Lorin  <https://orcid.org/0000-0002-7594-4634>
 Faith Vilas  <https://orcid.org/0000-0003-4723-5870>

References

- Bird, M. K., Volland, H., Howard, R. A., et al. 1985, *SoPh*, 98, 341
 Chashei, I. V., Bird, M. K., Efimov, A. I., Andreev, V. E., & Samoznaev, L. N. 1999, *SoPh*, 189, 399
 De Pontieu, B., Martínez-Sykora, J., & Chintzoglou, G. 2017, *ApJL*, 849, L7
 Gibson, S. E., & Low, B. C. 1998, *ApJ*, 493, 460
 Hollweg, J. V., Bird, M. K., Volland, H., et al. 1982, *JGR*, 87, 1
 Imamura, T., Tokumaru, M., Isobe, H., et al. 2014, *ApJ*, 788, 117
 Jensen, E. A., Frazin, R., Heiles, C., et al. 2016, *SoPh*, 291, 465

- Jensen, E. A., & Russell, C. T. 2008, *GeoRL*, **35**, L02103
- Kivelson, M. G., & Russell, C. T. 1995, *Introduction to Space Physics* (Cambridge: Cambridge Univ. Press)
- Klimchuk, J. A. 2006, *SoPh*, **234**, 41
- Levy, G. S., Sato, T., Seidel, B. L., et al. 1969, *Sci*, **166**, 596
- Mistry, R., Eastwood, J. P., Phan, T. D., & Hietala, H. 2015, *GeoRL*, **42**, 10513
- Odstroil, D., & Pizzo, V. J. 1999, *JGR*, **104**, 28225
- Scudder, J. D. 1994, *ApJ*, **427**, 446
- van Ballegooijen, A. A., Asgari-Targhi, M., & Berger, M. A. 2014, *ApJ*, **787**, 87
- Wei, F., Feng, X., Cai, H., & Zhou, Q. 2003, *JGRA*, **108**, 1238
- Whiting, C. A., & Spangler, S. R. 2009, EVLA Measurements Close To the Sun: Elevated System Temperatures, Tech. Rep., National Radio Astronomy Observatory, Expanded Very Large Array, Memo 136, <https://library.nrao.edu/evla.shtml>
- Yakovlev, O. I. 2002, *Space Radio Science* (New York: Taylor and Francis)